*5th International Symposium on Multiphase Flow, Heat Mass Transfer and Energy Conversion*
*Xian, China, 3–6 July 2005*

# Uniform Heat Transfer of Medical Cryogen Sprays through Wire Meshes

Walfre FRANCO[1], Hong HAN[1], Guo-Xiang WANG[2], and Guillermo AGUILAR[1*]

1. Laboratory of Transport Phenomena for Biomedical Applications
Department of Mechanical Engineering, University of California, USA
2. Department of Mechanical Engineering, University of Akron, USA

**Abstract.** Cryogen spray cooling (CSC) protects the epidermal layer during dermatologic laser surgery (DLS) of superficial vascular lesions. Because of spray characteristics the protection provided radially is relatively uniform only by the spray axis. The present work explores mass-deposition passive-control during CSC in order to increase the radial homogeneity of heat extraction. A stainless steel mesh is placed 5 and 10 mm away from the nozzle tip of the spray system, and a fast-response thermal sensor is used to measure temperatures across the radius of the sprayed surface of a human skin phantom. Surface measurements along with an analytical expression are used to compute heat fluxes. Lower temperatures and higher heat fluxes are obtained without the mesh. Consequently, the mesh quantitatively reduces cooling. However, radial distributions of temperature and heat flux show that more uniform heat transfer in time and space takes place using the mesh. Evolution of temperatures in time and space shows that the mesh introduces a thermal delay, which may be used to compensate for the reduction in cooling. Therefore, passive mass-deposition during CSC through a wire mesh effectively allows to establish a more uniform temporal and radial heat transfer.

## 1 Introduction

Superficial vascular lesions, such as hemangiomas and port wine stain (PWS) birthmarks, are congenital and progressive vascular malformations of the dermis. To remove them, laser energy is irradiated at appropriate wavelengths inducing permanent thermal damage to abnormal blood vessels. However, laser energy is also absorbed by epidermal melanin causing localized heating therein, and, if not controlled, complications such as hypertrophic scarring and skin dyspigmentation may occur. To prevent damage, epidermal protection is provided by means of cryogen spray cooling (CSC), which is a spatially selective heat transfer technique that spurts liquid cryogen onto the skin surface. Epidermal temperature decreases upon evaporation of liquid cryogen. Consequently, the laser fluence threshold for epidermal damage increases allowing the safe use of higher dosages [1]. Although CSC has been used for years and dramatically improved the therapeutic outcome of vascular lesions laser surgery, there are still many clinical, optical and heat and mass transfer limitations in current procedures. For instance, the inability of CSC to provide uniform-radial epidermal protection.

Heat removal from skin during CSC is a function of many fundamental spray parameters—such as average droplet diameter and velocity, mass flow rate, temperature and spray density among others [2, 3]—that vary in time and space within the spray cone. Therefore, heat extraction from skin during CSC-assisted dermatologic laser surgery (DLS) is non uniform [4, 5]. Uniform heat extraction for epidermal protection within the sprayed area is highly desirable. In previous studies we have experimentally addressed the radial and temporal evolution of heat transfer during CSC, and found that cooling is uniform radially within 2 mm of an 8 mm radius of the sprayed surface of a skin phantom [6]. In further studies, these measurements were used as boundary conditions of a mathematical model of CSC-DLS for PWS therapy to study effects of radial variations in cooling on epidermal protection; it was found that, at the end of a 60 ms spurt there are large temperature differences along the radial and depth coordinates within the epidermis, such that a 0.45 ms laser pulse at 585 nm and 5 J/cm$^2$ caused irreversible damage therein. A 60 ms delay between end of spurt and laser onset was successfully introduced to allow for a more homogeneous temperature distribution and, consequently, overcome skin damage in this particular procedure [7]. In order to enhance epidermal protection, our research group has carried out several investigations, such as control of cryogen deposition, for which results showed that wire meshes—placed in between the spray nozzle and cooling surface—reduce heat extraction efficiency and prolong cooling duration in the center of the sprayed surface [8].

## 2 Objective

The aim of the present work is to investigate temporal and radial variations in surface cooling of a skin phantom during mass-deposition passive-control of CSC, specifically,

*Address all correspondence to this author: gaguilar@ucr.edu

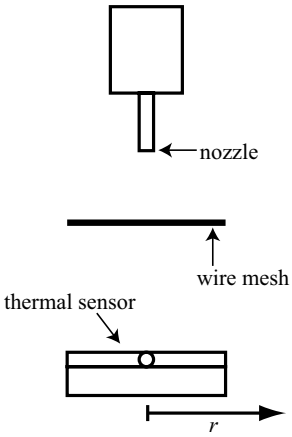


Fig. 1. Experimental set up.

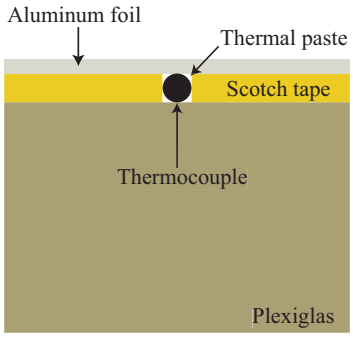


Fig. 2. Fast-response temperature sensor.

Table 1. Thermal properties of epidermis [9] and sensor components [10].

| | $c$ [J/kg K] | $\rho$ [kg/m$^3$] | $k$ [W/m K] |
|---|---|---|---|
| epidermis | 3600 | 1200 | 0.21 |
| Plexiglas® | 1300–1500 | 1150–1190 | 0.19–0.24 |
| Al foil | 896 | 2710 | 205 |
| Scotch tape® | 1400 | 1280 | 0.22 |

through the use of a wire mesh.

## 3 Experimental and Numerical Methods

Temporal and radial profiles of surface temperature are experimentally obtained with and without wire mesh. Experimental data along with an analytical solution—based on Fourier's law of heat conduction and Duhamel's theorem of superposition—are used to calculate surface heat fluxes. Next, surface heat transfer with and without mass-deposition control is compared to assess relative merits and disadvantages of each case. Finally, a discussion about the implications of using wire meshes in CSC-assisted DLS is presented.

### 3.1 Cryogen spray system

Liquid cryogen R-134a, with a boiling temperature at atmospheric pressure of $T_b \approx -26$ °C, is delivered to a fuel injector attached to a straight-tube nozzle with inner diameter $d = 1.4$ mm and length $l = 55.6$ mm. The spray system is electronically controlled and set to deliver 60 ms single cryogen spurts. The nozzle is positioned 40 mm away from the human skin phantom.

### 3.2 Mass deposition control

To control the deposition of liquid cryogen, a stainless steel wire mesh of size 400 (9231744 McMaster-Carr, Los Angeles CA) is placed among the sensor surface and nozzle tip at 5 and 10 mm from the nozzle tip. A scheme of the experimental set up is shown in Fig. 1. The mesh is allowed to dry before each spurt in order to avoid water condensation and freezing on the mesh.

### 3.3 Skin model and thermal sensor

A fast-response thermal sensor—similar to that proposed by Aguilar et al. [11]—is placed on top of a Plexiglas substrate. The sensor is schematically shown in Fig. 2. A miniature type-K thermocouple is placed on top of a 6 mm thick polymethyl methacrylate (Plexiglas®) bar, and a 0.5 mm thick cellulose tape (Scotch tape®) is placed next to the thermocouple bead to fill the gap between aluminum and human skin phantom. According to the manufacturer, the time constant of the thermocouple bead is $\approx 2$ ms. A piece of aluminum foil ($15 \times 10$ mm surface and $L = 0.2$ mm thickness) covers the sensor, and thermal paste around the thermocouple bead is used to ensure good thermal contact. This temperature sensor provides a substrate with thermal properties similar to human skin such that their thermal responses are comparable. Thermal properties of epidermis and sensor components are shown in Table 1.

The temperature of the thermal sensor at room conditions is $\approx 21$ °C. Initially, the thermocouple bead is placed at the center of the spray cone and, subsequently, it is displaced using a BiSlide® positioning system (Velmex Inc., Bloomfield NY) to measure temperatures every 1 mm from the center, $r = 0$ mm, to the periphery of the sprayed surface, $r = 8$ mm. Independent runs with fixed parameter values showed good experimental repeatability. Temperature is acquired through an A/D converter (instruNet, GW Instruments Inc., Sommerville MA) hardware and LabView software (National Instruments, Austin TX) at 2000 Hz, and noise is filtered out by averaging 30 adjacent points.

### 3.4 Heat transfer computations

Time, depth and length scales in laser therapy assisted by CSC allow the heat transfer to be modeled as a one-dimensional heat diffusion problem with known surface temperature [11, 12]. The material thermal diffusivity $\alpha$ is defined as the ratio of thermal conductivity $k$ to density $\rho$ and specific heat $c$, i.e., $\alpha = k/(\rho c)$. For the aluminum foil, the

thermal diffusion time is $L^2/\alpha \approx 5\times10^{-6}$ s, and the Biot number [10], $hL/k$, for a typical heat transfer coefficient of spray, $h \simeq 10000\,\mathrm{W/m^2K}$ [10], is $\approx 1\times10^{-3}$. Since $Bi << 1$, the temperature of the foil is assumed to be spatially uniform in the vicinity of the thermocouple bead. If the surface temperature is known, a direct heat conduction problem for the temperature distribution within the substrate may be solved to determine the temperature gradient at the surface and, subsequently, the surface heat flux from Fourier's law. Alternatively, Duhamel's theorem can be used to evaluate the temperature gradient at the surface if thermal properties remain constant. Both methods provide nearly identical solutions, however, the latter is used herein since it is easier to implement numerically.

Duhamel's theorem is based on the principle of superposition and states that the substrate thermal response at $t$ equals the total sum of what the substrate experienced in small steps prior to $t$ [13–15]. For constant thermal properties, the temperature form of Duhamel's theorem is

$$\theta(z,t) = \theta_o + \int_{t_o}^{t} u(z,t-\tau)\frac{dT}{d\tau}d\tau, \tag{1}$$

where $\theta$ is the substrate temperature, $\theta_o$ is the uniform initial temperature, $u$ is the temperature response function of the substrate (initially at zero temperature) to a unit step in surface temperature, $z$ is the coordinate perpendicular to the surface, $t-\tau$ is the time that has elapsed since the step at $\tau$, and $T$ is the surface temperature [13, 16]. Using Eq. 1, Fourier's law [10], for a continuous surface temperature in time, can be written as

$$q(t) = -k\frac{\partial\theta}{\partial z}, \tag{2}$$

$$= -k\int_{t_o}^{t}\frac{\partial u(z,t-\tau)}{\partial z}\frac{dT}{d\tau}d\tau, \tag{3}$$

where partial derivatives are evaluated at the surface ($z=0$). The unit step function for a semi-infinite planar solid is

$$u(z,t) = 1-\mathrm{erf}\left(\frac{z}{2\sqrt{\alpha t}}\right), \tag{4}$$

then

$$\partial u/\partial z = -1/\sqrt{\pi\alpha t}, \tag{5}$$

[14, 15]. Substituting Eq. 5 in 3 the surface heat flux can be written as

$$q(t) = \sqrt{\frac{k\rho c}{\pi}}\int_{t_o}^{t}\frac{1}{\sqrt{t-\tau}}\frac{dT}{d\tau}d\tau. \tag{6}$$

Assuming that the surface temperature is measured at discrete times $t_i$ and that the surface temperature varies linearly in time between successive times, Eq. 6 can be integrated analytically to obtain

$$\hat{q}_I = 2\sqrt{\frac{k\rho c}{\pi}}\sum_{i=1}^{I}\left(\frac{T_i-T_{i-1}}{t_i-t_{i-1}}\right)\left(\sqrt{t_I-t_{i-1}}-\sqrt{t_I-t_i}\right), \tag{7}$$

$$= 2\sqrt{\frac{k\rho c}{\pi}}\sum_{i=1}^{I}\frac{T_i-T_{i-1}}{\sqrt{t_I-t_i}+\sqrt{t_I-t_{i-1}}}, \tag{8}$$

where $\hat{q}$ is the approximate surface heat flux for a semi-infinite planar body. A more detailed discussion about this approximation can be found in references [6, 15]. For simplicity, $\hat{q}$ is written as $q$ in the following sections.

## 4 Results and Discussion

In this section, surface temperature $T$ represents the average value of two independent measurements, and surface heat flux $q$ are computed using $T$. As shown in [6], the cryogen spray is very stable, thus, the experiment repeatability is also very good.

### 4.1 Temporal evolution of heat transfer

Dynamics of $T$ without and with mesh are shown in Fig. 3. The arrow in each subfigure indicates the correspondence between measurements and radial location, that is, the bottom curve corresponds to $T$ at $r=0$ mm while the top one to $T$ at $r=8$ mm. At $t=0$ ms, every location is at 21 °C (room temperature), and, as the spray reaches the surface, each location experiences a different cooling rate because of radial variations in the spray characteristics, such as particle size and velocity of the impinging cryogen droplets. Note that the difference in surface temperature between $r=0$ and 8 mm increases during heat extraction, and, subsequently, decreases as the skin phantom goes back to thermal equilibrium. Without mesh, Fig. 3(a), at $t\approx100$ ms, temperature values at each location are similar except for the three outermost (which correspond to $r=6$, 7 and 8 mm; i.e., the three curves on top). Similarly, with the mesh at 5mm and 10 mm, Figs. 3(b) and (c), at $t\approx200$ and 250 ms respectively, temperature values at each location are similar except for the same three outermost locations. Note also that the period of time with similar temperatures is larger with the mesh at 10 mm than without it. This illustrates that the wire mesh certainly has an effect on the temporal and radial distributions of the spray. Without mesh, Fig 3(a), the overall minimum surface temperature $T_{min}\approx-40$ °C (68 ms) occurs by the center of the sprayed surface, which coincides with the center of the spray. With the mesh, $T_{min}\approx-32$ (72 ms) and -30 °C (71 ms) for 5 and 10 mm, respectively. It follows that the mesh limits reduction of temperatures by the center of the spray.

Dynamics of $q$ without and with mesh are shown in Fig. 4. The arrow in each subfigure indicates the correspondence between computations and radial location, that is, the top

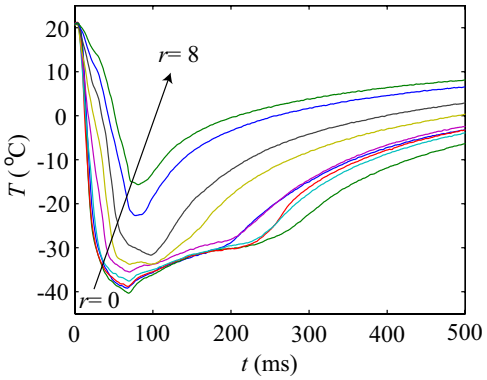


(a) No mesh

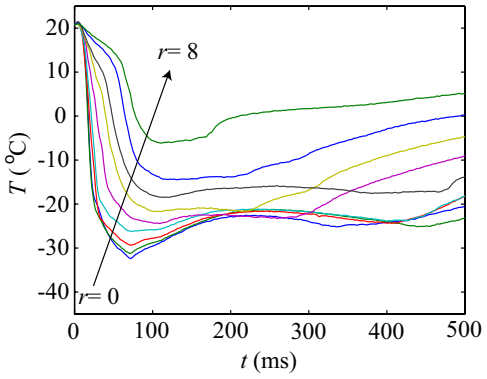


(b) Mesh at 5 mm from nozzle tip

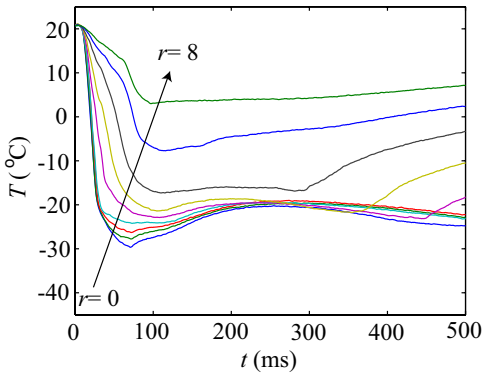


(c) Mesh at 10 mm from nozzle tip

Fig. 3. Temporal evolution of surface temperature.

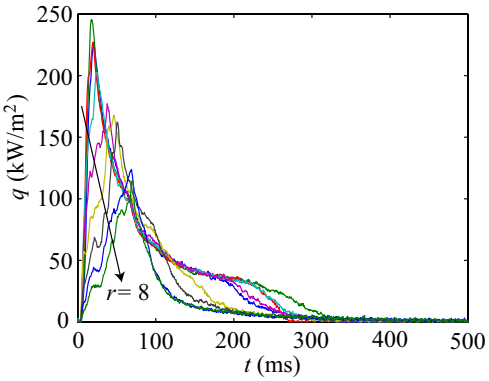


(a) No mesh

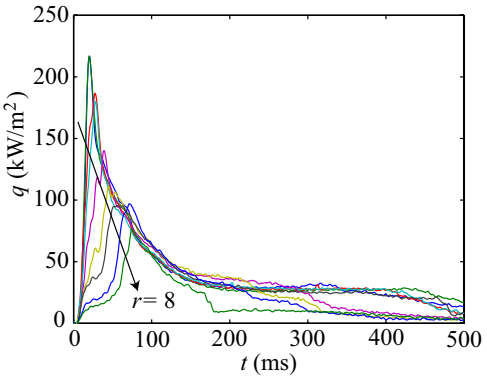


(b) Mesh at 5 mm from nozzle tip

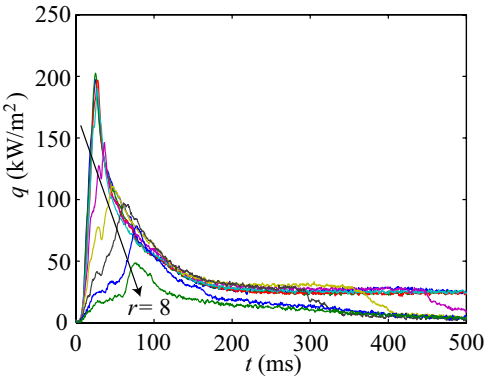


(c) Mesh at 10 mm from nozzle tip

Fig. 4. Temporal evolution of surface heat flux.

curve corresponds to $q$ at $r = 0$ mm while the bottom one to $q$ at $r = 8$ mm. At $t = 0$ ms, the skin phantom is in thermal equilibrium, and, as the spray reaches the surface, a heat flux between the skin phantom and surroundings occurs. Because of the difference in cooling rates between radial locations, the greatest $q$ occurs by the center of the sprayed area without and with mesh. Without mesh, Fig. 4(a), the difference in maximum heat flux, $q_{max}$, between the center and perimeter of the sprayed surface is 80 kW/m$^2$, and the time of occurrence of $q_{max}$ varies from one location to another: the farther from the center, the later $q_{max}$ occurs. With the mesh at 5 and 10 mm, Figs. 4(b) and 4(c), the difference in $q_{max}$ between center and perimeter is 142 and 148 kW/m$^2$, respectively. The overall $q_{max}$ occurs without mesh for which the heat extraction is over at 300 ms, whereas with the mesh the heat extraction goes on beyond 500 ms. Therefore, the mesh reduces quantitatevely the surface heat extraction in every location but extends it in time.

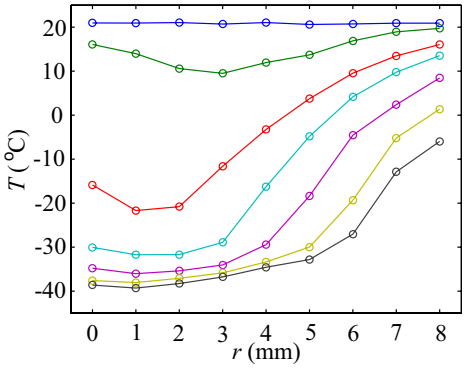


(a) No mesh

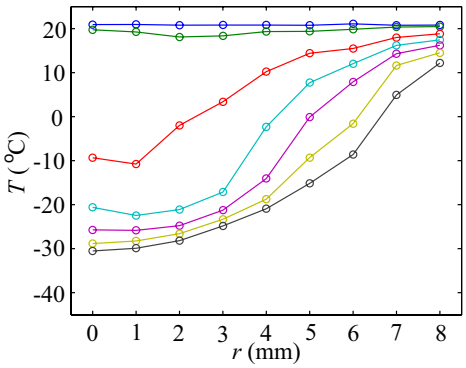


(b) Mesh at 5 mm from nozzle tip

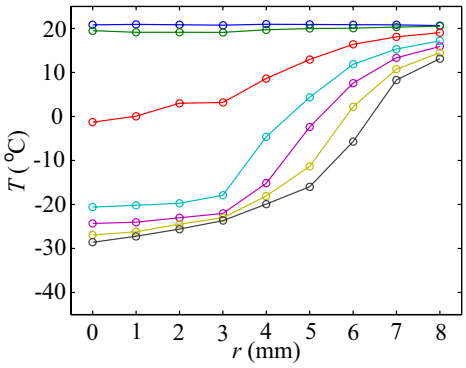


(c) Mesh at 10 mm from nozzle tip

Fig. 5. Radial evolution of surface temperature.

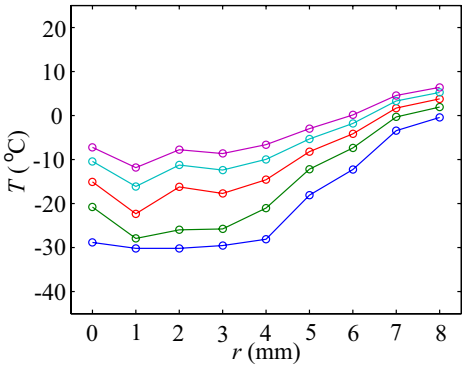


(a) No mesh

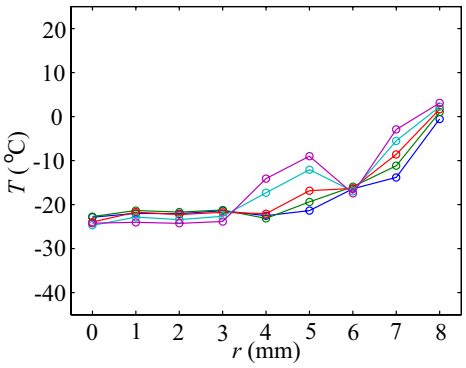


(b) Mesh at 5 mm from nozzle tip

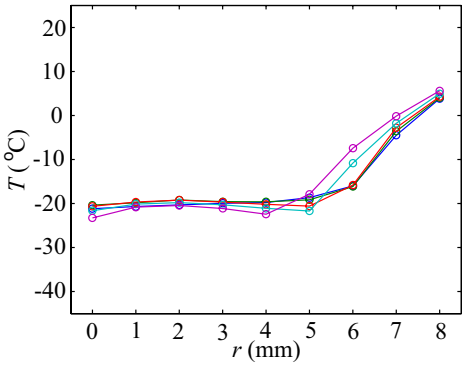


(c) Mesh at 10 mm from nozzle tip

Fig. 6. Radial evolution of surface temperature.

### 4.2 Radial evolution of heat transfer

$T$ as a function of $r$ for specific times without and with mesh is shown in Fig. 5. Curves are drawn every 10 ms from $t = 0$ (top curve) to 60 ms (bottom curve). The bottom curve in each subfigure corresponds to the end of the spurt, at this time $T$ is uniform radially in Fig. 5(a) within a 4 mm radius—where the difference in temperatures among the center and other locations is less than 5 °C—and in Figs. 5(b) and (c) within a 3 mm radius. Radial distributions of $T$ every 50 ms from $t = 200$ to 400 ms are shown in Fig. 6. In Fig. 6(a), curves at the bottom and top correspond to 200 and 400 ms, respectively; that is, the heat extraction process is ending and the skin phantom is going back to thermal equilibrium with the surroundings. Note that in Figs. 6(b) and (c) more uniform temporal and radial distributions are induced by the mesh. Indeed $T$ is uniform radially in the 10 mm case, Fig. 5(a), within a 5 mm radius.

Radial profiles of $q$ for specific times without and with mesh are shown in Fig. 7. Curves are drawn in 2 ms intervals from 0 (bottom curve) to 20 ms (top curve) in Figs. 7(a) and 7(b), and from 0 to 26 ms in Fig. 7(c). These are the approximate times when each $q_{max}$ occurs. In each case $q_{max}$ occurs early in time—before the spurt is over. $q$ is more homogeneous radially when the mesh is at 10 mm.

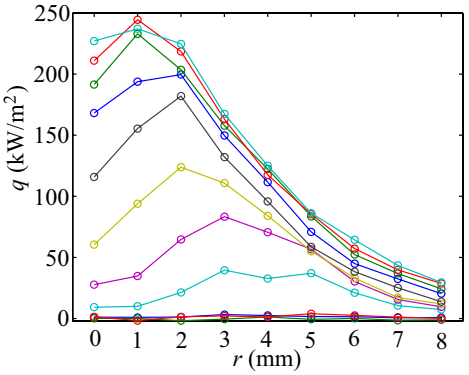


(a) No mesh

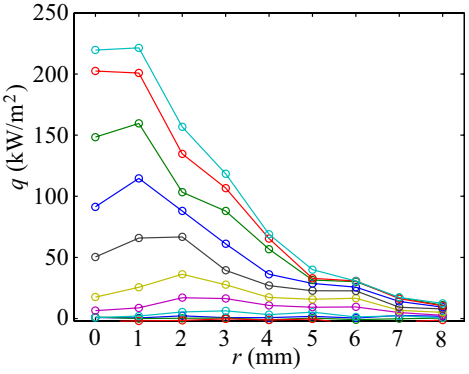


(b) Mesh at 5 mm from nozzle tip

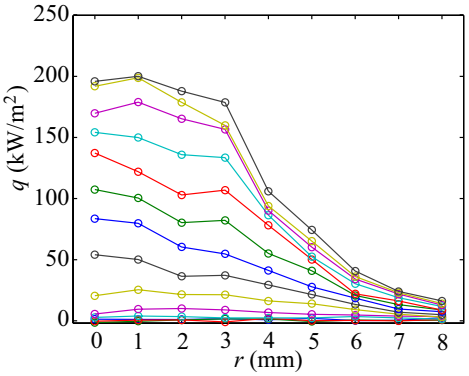


(c) Mesh at 10 mm from nozzle tip

Fig. 7. Radial evolution of surface heat flux.

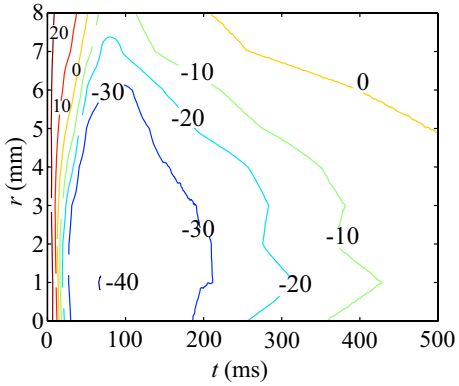


(a) No mesh

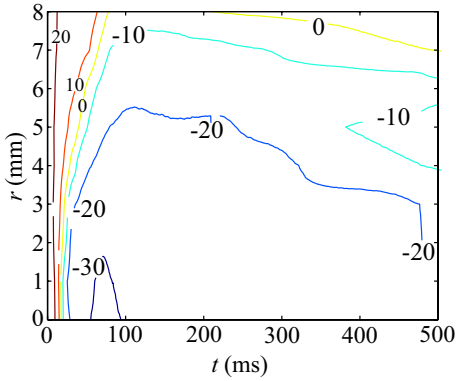


(b) Mesh at 5 mm from nozzle tip

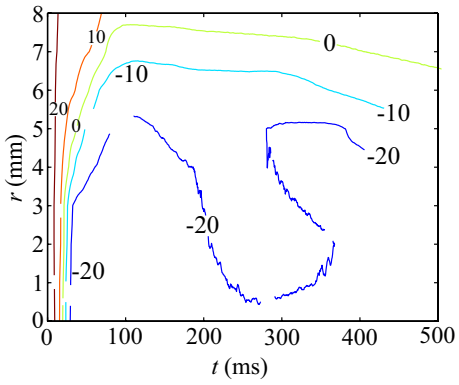


(c) Mesh at 10 mm from nozzle tip

Fig. 8. Temporal and radial evolution of surface temperature.

### 4.3 Temporal and radial evolution of heat transfer

Isotherms in time and space without and with mesh are shown in Fig. 8. The more uniform $T$ is radially, the more straight the isotherm is. By comparing isotherms among subfigures it can be observed that the largest radius of uniform $T$ is $\approx 6$ mm at $t \approx 100$ ms without mesh, Fig. 8(a). Considering the area enclosed by the isotherm at 20 °C in the 5 mm case, Fig. 8(b), there is a region of uniform temperature starting at $\approx 150$ ms with a 5 mm radius and ending at $\approx 450$ ms with a 3 mm radius—see also Fig. 3(c). A similar observation can be made in the 10 mm case, Fig. 8(b), where the region of uniform temperature starts at $\approx 150$ ms with a 5 mm radius and ends at $\approx 450$ ms with a 4 mm radius; the 20 °C isotherm in this figure is somehow misleading because the temperature is oscillating at this value but the same observation can be made in Fig. 3(b).

### 4.4 Discussion

Dynamics of surface temperature $T$ and heat flux $q$, Figs. 3 and 4, show that lower minimum temperature $T_{min}$ and higher maximum heat flux $q_{max}$ are obtained overall by the

center of the spray without a mesh. A previous study that measured temperatures only at the center of the spray reported the same observation [8]. Radial profiles of $T$ and $q$, Figs. 6 and 7, show that the wire mesh at 5 and 10 mm effectively produces more radial-uniform heat transfer.

Using the wire mesh at 10 mm from the nozzle tip—with the spray system described herein—during cryogen spray cooling (CSC) would result in a quantitative reduction of surface cooling but a more uniform cooling in time and space, respect to CSC without mesh. As a result, less deep but more uniform epidermal protection would be supplied with the mesh, provided the cooling time periods are the same. The reduction in cooling may be due to a loss in momentum and gain in temperature of cryogen droplets going through the mesh: several droplets impact the mesh changing the average velocity field and, because the mesh is at room temperature, increasing the temperature of the spray. Droplets also break and collisions may increase at the mesh. Consequently, the average diameter distribution is also affected. Temporal and radial evolutions of the temperature field, Fig. 8(a)–(c), show that the mesh introduces a thermal delay since the same isotherms develop at different times. Certainly, there are some limit values that will never be reached with the mesh. Nevertheless, a time delay between the end of the spurt and the onset of laser irradiation may be used to compensate for the quantitative reduction in cooling. Figures 6(a)–(c) illustrate which temperatures at the center of the sprayed surface can be reached by introducing a delay when using the mesh. As reported in similar studies, the time delay between CSC and laser irradiation is fundamental for maximizing epidermal protection [5].

## 5 Conclusions

Mass-deposition control during CSC through wire meshes effectively allows to homogenize radial heat transfer, and, by appropriate readjustment of the time lapse between spurt termination and laser irradiation onset, to increase the homogeneity in heat extraction. Mass-deposition control amplifies the time period and radius of uniform cooling reducing the risk of epidermal damage at the laser beam periphery during the treatment of patients.

## 6 Acknowledgment

This work was supported in part by the National Institutes of Health (HD42057 to GA and AR47551 to JSN). Research support by Henry Vu is greatly appreciated.

## 7 References

[1] J S Nelson, T E Milner, B Anvari, B S Tanenbaum, S Kimel, L O Svaasand, and S L Jacques. Dynamic epidermal cooling during pulsed-laser treatment of port-wine stain - a new methodology with preliminary clinical evaluation. *Arch. Dermatol.*, 131(6):695–700, 1995.

[2] G. Aguilar, B. Majaron, K. Pope, L. O. Svaasand, E. J. Lavernia, and J. S. Nelson. Influence of nozzle-to-skin distance in cryogen spray cooling for dermatologic laser surgery. *Lasers Surg. Med.*, 28(2):113–120, 2001.

[3] E Karapetian. Influence of cryogenic spray parameters on surface heat extraction on human skin. Master's thesis, Department of Chemical Engineering and Materials Science, University of California, Irvine, CA, 2002.

[4] W Franco, G X Wang, E Karapetian, J S Nelson, and G Aguilar. Effect of surface thermal variations during cryogen spray cooling in dermatologic laser therapy. In *Proc. ILASS Americas*, 2004. 17th Annual Conference on Liquid Atomization and Spray Systems.

[5] W Franco, G X Wang, J S Nelson, and G Aguilar. Radial heat transfer dynamics during cryogen spray cooling. In *Proc. ASME International Mechanical Engineering Congress*, 2004. IMECE2004-59609.

[6] W Franco, J Liu, G X Wang, J S Nelson, and G Aguilar. Radial and temporal variations in surface heat transfer during cryogen spray cooling. Phys. Med. Biol., 50:387–397, 2005.

[7] W Franco, R Zhang, J S Nelson, and G Aguilar. Numerical modeling of spray cooling-assisted dermatologic laser surgery for treatment of port wine stains. In *Proc. SPIE International Symposium, Photonics West*, 2005. 5686A-19.

[8] H Vu, G Aguilar, and J S Nelson. Passive mass deposition control of cryogen sprays through the use of wire meshes. *Lasers Surg. Med.*, 34(4):329–334, 2004.

[9] F A Duck. *Physical properties of tissue*. Academic press, London, 1990.

[10] FP Incropera and DP Dewitt. *Fundamentals of heat and mass transfer*. Wiley, New York, 1996.

[11] G Aguilar, G X Wang, and J S Nelson. Dynamic behaviour of cryogen spray cooling: effects of spurt duration and spray distance. *Lasers Surg. Med.*, 32(14):152–159, 2003.

[12] M J C van Gemert and A J Welch. Time constants in thermal laser medicine. *Lasers Surg. Med.*, 9(4):405–421, 1989.

[13] H S Carslaw and J C Jaeger. *Conduction of heat in solids*. Oxford University Press, London, 1959.

[14] M N Özişik. *Heat Conduction*. Wiley, New York, 1980.

[15] J V Beck, B Blackwell, and J R St. Clair, Jr. *Inverse heat conduction: ill posed problems*. Wiley, New York, 1985.

[16] G E Meyers. *Analytical methods in conduction heat transfer*. McGraw Hill, New York, 1971.